Neural Computing and Applications (2023) 35:14551–14564
https://doi.org/10.1007/s00521-021-06301-2

S.I: ML4BD_SHS

A machine learning-enabled intelligent application for public health and safety

Zhang Yong[1] · Zhang Xiaoming[2] · Mohammad Dahman Alshehri[3]

Received: 26 January 2021 / Accepted: 1 July 2021 / Published online: 11 August 2021

Abstract

This article uses a machine learning approach to analyze and detect burst signals in a smart healthcare system to protect and safeguard the public health. We consider the time-series electrocardiogram (ECG) waveforms for the detection of burst signals. For this purpose, we propose an intelligent differential correlation burst detection (DCBD) approach by establishing a mathematical model and deriving the analytical expressions to detect false alarm rate and missed detection rate in ECG signals. DCBD feeds the burst signals of a large-scale ECG waveform into various filters for noise removal, which are then passed through data augmentation to achieve high specificity and sensitivity. These waveforms are then segmented for feature extraction and machine learning (ML) classification. Finally, burst-free ECG waveforms are broadcast to a database server, where ML algorithms are used to detect the presence of any abnormal activities. Furthermore, the ECG signal is classified to a set of heart diseases using the well-known LSTM (Long Short-Term Memory) and CNN (Convolutional Neural Network) models. Our proposed approach highlights that the probability of false alarm rate is similar to that caused by pure noise within the ECG waveforms. Our evaluation, using numerical experiments, suggests that the accuracy of the LSTM based ECG signal classification could be approximately 11.7% and 12.8% improved, subsequently, using the proposed burst detection method.

Keywords Smart healthcare system · Machine learning · Burst detection · False alert rate · Missed detection rate · Public safety

1 Introduction

At present, the electromagnetic environment is becoming increasingly complex. The limitations of existing technologies along with competing devices for scarce spectrum result in an extremely low Signal-to-Noise ratio (SNR) for non-cooperative received signals [1]. These limitations bring numerous challenges, particularly, in healthcare system where signals are used to detect certain types of heart diseases. Among them, burst noise, i.e., burst signals, is a major concern due to the inconsistent transmission medium [2], which may essentially affect the accuracy of the healthcare system and may lead to fatalities. In addition, due to the concealment and short duration of burst communication transmission, the ability to resist reconnaissance and interception is very strong, making the detection of burst signals extremely difficult. Due to the increasingly fierce competition for spectrum resources, the number of devices in the same frequency band has increased exponentially, making the detection performance of traditional approaches (under low SNRs) unable to meet the constantly updated demands and performance guarantees of contemporary communications [1].

With the emergence of Internet of Things (IoT), the competition for scarce spectrum has increased at an exponential scale [3]. IoT enables every physical device to participate in network communication that increases the competition for channel allocation in the same frequency

✉ Zhang Yong
yongzhang@hbue.edu.cn

[1] School of Finance and Public Administration, Hubei University of Economics, Wuhan, China

[2] Department of Vehicle Engineering, Academy of Army Armored Forces, Beijing, China

[3] Department of Computer Science, College of Computers and Information Technology, Taif University, P.O. Box 11099, Taif 21944, Saudi Arabia

band. Among the applications of IoT, smart healthcare system has found its acceptance worldwide due to its patient-centric approach and sensitivity of medical data. In a smart healthcare system, a huge number of devices are involved in data transmission to provide seamless and interoperable communication. The large-scale deployment of these devices is subject to scarce spectrum availability at the physical layer [4]. As a result, the data are subject to excessive noise, distortion and attenuation which may have undesirable consequences if these issues are left unattended. The availability of limited spectrum and error-prone channels causes signal burst that requires urgent attention as it is a constant threat to public safety and security [5]. With the advent of healthcare-compatible communication technologies, data collection and transmission among the devices suffer relatively lower SNR as these technologies rely on cooperative communication mode. However, with the increase in sensing equipment and the integration of heterogeneous communication approaches, the multipath effect is added to the transmitted signal. As a result, the performance of wireless communication systems for healthcare technologies has dropped sharply. Hence, more theoretical research is focused on modulation recognition nowadays, but the prerequisite for communication modulation is signal detection [6, 7]. The signal burst detection process uses time division multiple access (TDMA) slots that contain a sequence of bits or symbols, which are difficult to recognize. Its design purpose is to complete data assisted (DA)-based burst detection synchronization because data-assisted approaches have better performance.

At present, many different approaches for burst detection are based on data-related operations. Simple correlation is one of the most direct detection approaches and is widely used for burst detection. Moreover, ML-based Symbol Timing Offset Estimation (STOE) for burst signals is another well-known detection approach [8]. When this approach is used for frame synchronization, the SNR required to achieve the same performance is lower than the simple correlation approach by more than 3 dB. The ML-approach is further extended to adapt to MPSK signal modulation [16]. However, when there is a frequency offset, the performance of the ML-approach drops sharply. For this reason, the Ref [17] proposed a novel approach of segment correlation to decrease the influence of frequency offset, but when the frequency offset is large, the performance of this approach still decreases significantly. In order to solve this problem, the Refs [18–20] used a more general signal model to further improve the ML approach and achieved good results. However, this approach aimed at frame synchronization (that is, by finding the corresponding likelihood the time position of the detection volume is synchronized) designed. For burst detection, Refs [21, 22] proposed a simple correlation-based constant false alert (CFAR) method and analyzed its theoretic performance. The analysis results show that these approaches cannot adapt to large frequency deviations. In the Refs [23–25], the author proposed the ALRT technique, which can effectively overcome the adverse effects of frequency offset. In this technique, the detection expression includes differential correlation calculation, which makes the frequency offset robust, which causes the setting of the detection threshold to rely on experience. In addition, it must be pointed out that the modulated signal part with information is the same as the noise part, which will cause false alerts in burst detection. However, the existing research only considers the false alerts caused by the noise part and ignores the false alerts caused by the modulated information signal part. False alerts make the analysis of detection performance incomplete. At present, there have been many researches on the detection technology of burst signals, which are mainly divided into time domain detection algorithms and frequency domain detection algorithms. Time domain detection algorithms include short-term energy way, autocorrelation technique, high-order cumulate, and optimal fitting. Degree way, singular value decomposition way, etc.; frequency domain detection algorithms mainly include Power-Law algorithm based on DFT, Power-Law algorithm based on high-order spectrum, spectral entropy way, etc.

The first step is burst detection for the burst signal interception and demodulation. In this paper, we analyze the performance for the DCDB theoretically and the analytical expressions of the performance of disappeared detection rate and artificial alert rate are derived. Different from the previous studies, the false alert caused by the signal part of the message is considered, and it is proved that the false alert probability is similar to that caused by pure noise. According to the results, we know that the characteristics of the detection rate are summarized. By simulation, we come to the conclusion that the performance of DCBD is not affected by frequency offset. The second step is to accurately classify the ECG signal for further analysis and disease detection. Each class with its corresponding ECG pattern signal is pre-defined. Some trends can be visually detected easily in each class, distinguishing the signals belonging to each class. Different forms of dysfunctionality that can affect the human heart are defined by the classes given. In the database referred to in the previous section, they were chosen according to their availability. The first class involves documenting, in sinus rhythm and during a resting state, of subjects that are all well. The subjects came from various groups of age and had good records of heart disorders of the past. Patients diagnosed with Congestive Heart Failure 4 (CHF) and Extreme Congestive Heart Failure were in the second class

[25]. This is a disorder in which the amount of blood circulation in the heart fails to satisfy the needs of the body. There are ECG recordings of people with heart arrhythmia in the third level, or also known as cardiac dysrhythmia. This dysfunction of the heart is identified by an irregular rhythm in a heartbeat: a beat that has been missed, an extra beat, a fluctuation in the rate or a very fast/slow beat and vice versa.

The analysis provides a reference for how to set the detection threshold to satisfy the detection function requirements under different signal conditions. The analysis of the theoretic performance of burst detection is helpful to assess the system function and guide how to set the detection threshold under different signal conditions. Different from the previous studies, the false alert caused by the signal part of the message is considered, and it is proved that the false alert probability is similar to that caused by pure noise. By the theoretical analysis, we have that the characteristics of the detection way are summarized, and the setting way of detection threshold is given.

The rest of the paper is organized as follows: In Sect. 2, we proposed the system model for the intelligent machine learning-based healthcare system. In Sect. 3, an approach to remove the burst or noise from the signal is presented. Section 4 sheds light over two machine learning models in order to classify the refined ECG signal to an appropriate heart disease category. We study the performance of the proposed system (burst detection and deep learning methods), using real datasets, and discuss the obtained outcomes in Sect. 5. Finally, Sect. 6 concludes this article along with future research directions.

2 System model of our proposed approach

In this section, we present the system model of our proposed differential correlation approach for burst detection in a smart healthcare system. In Fig. 1, the burst of ECG signal at the physical layer is evaluated. The ECG sensors embedded to the patient gather vital electric signals from the patient's heart to examine heart conditions. The continuous waveforms of ECG signals are subject to burst noise present at the transmission channels. The noise affects the wavelength and frequencies of the ECG signals. As a result, the vital information within the ECG waveforms are corrupted that may have catastrophic effect in any IoT-enabled healthcare system and may disrupt the public safety and health. In worst case, the transmission of corrupted and inaccurate information of a patient' heart condition to a practitioner may lead to fatality. To detect the burst noise, we propose a differential correlation detection using filters, augmentation, segmentation, and machine learning algorithms.

The time-series continuous waveforms of ECG sensors experience too much burst noise due to the presence of inconsistent transmission medium. We remove the noise using matched and shaping filters. Next, data augmentation is applied that increases the number of data points. In case of ECG signals, data augmentation increases the number of images, which ensures higher specificity and sensitivity. After augmentation, we create segments of ECG signals. In this case, we create seven segments: one normal and six abnormal segments of the ECG signal. These segments are important for feature extraction and machine learning classification. Besides, any outlier present is detected and ultimately removed. Finally, the burst-free data are transmitted to the IoT gateway which is routed toward the IoT web and database server. At this stage, Machine Learning (ML) algorithms are used for classification to detect the presence of any abnormal activities [11, 12]. We assume a set of pre-defined heart diseases signals and train the model over the received signals (refined i.e., no burst) to classify the patient heart activity. Upon ML classification, the highly refined data are available for visualization, alert generation and reporting to the practitioners. The machine learning based approaches including LSTM and CNN models are further described in Sect. 4.

3 Differential correlation for burst detection in a smart healthcare system

We assume that the propagation channel for ECG waveform is an Additive White Gaussian Noise (AWGN) channel. The TDMA signal of one-time socket is converted into baseband and then processed by matched filtering using Eq. 1.

$$S_n = Ae^{j(\Omega \pi r_1 + \theta)} \sum_i d_i h(nT_s - kT - \tau) + v_n \quad n \in [0, (L-1)P] \tag{1}$$

In this equation, A represents amplitude of the signal, Ω_o denotes the frequency offset, θ is the initial phase of the signal, d_i represents the data symbol, $h(t)$ represents the shaping filter, T_s represents the sampling interval of a symbol, T represents the sign time, $P = T/T_s$ is the oversampling element, τ is a delay factor, v_n is the compound-added White Gaussian Noise (WGN), σ^2 represents the variance, L is the count of symbols contained within the TDMA socket.

In our proposed approach, we set the time of TDMA burst mainly for burst detection. The detection can be implemented by sliding the window in the signal, and the window length can be set as the length of the leading head. Once the detection rate exceeds a predetermined threshold, it means that the burst has been examined. Otherwise, the

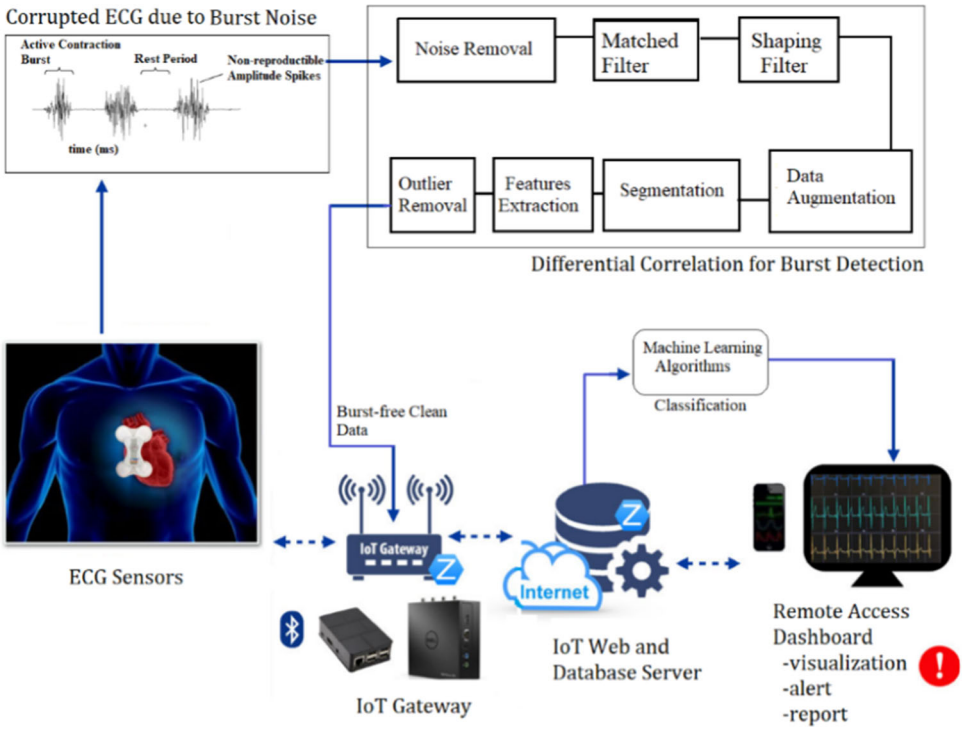

Fig. 1 System model of our proposed approach

detection window will slide a sample to continue the detection procedure. To simplify the calculation, the samples in the detection window can be extracted according to the symbol period. In other words, only the samples in the set $\{r_i = s_i p + \mu | i = 0, \ldots, L-1\}$ are used to calculate the detection quantity.

Definition: H_1 represents the leading signal sample in the detection window, namely

$$H_1 : r_i = Ae^{j(\omega_0 i+\theta)}(c_i h(\mu T_s - \tau) + \sum_{k\neq i} c_k h(i-k)T + \mu_0 T_s) - \tau)) + v_i, \quad i = 0, \ldots, N-1 \tag{2}$$

where, c_i is the given leader sequence, $\omega_0 = \Omega_0 T$ is the normalized rate of recurrence offset, and N is the size of detection window. If the oversampling value is too big, the value of b will be small, and the inter-symbol interference is relatively weak and needs to be ignored. At this point, we can redefine H_1 using Eq. 3.

$$H_1 : r_i = Ae^{j(\omega_0 i+\theta)}c_i + v_i, \quad i = 0, \ldots, N-1 \tag{3}$$

In our proposed approach, the ECG signals may have false alarms originating from the noise segment. For this purpose, we define $H_{0,0}$ as the signal gap, i.e., the noise segment, as shown in Eq. 4.

$$H_{0,0} : r_i = v_i, \quad i = 0, \ldots, N-1 \tag{4}$$

Next, we define $H_{0,1}$ to represent the message signal in the detection window, using Eq. 5.

$$H_{0,1} : r_i = Ae^{j(\omega_0 i+\theta)}d_i + v_i, \quad i = 0, \ldots, N-1 \tag{5}$$

Here, d_i represents the message symbol, which is equally distributed within the modulation symbol set. Please note that each message denotes a waveform of the ECG signal.

We derive the burst detection algorithm with the maximum likelihood test ratio and differential correction. The likelihood ratio of a sudden detection problem for an ECG waveform can be expressed using Eq. 6.

$$L(r|\theta, \omega_0, d) = \frac{p_1(r|\theta, \omega_0)}{p_0(r|\theta, \omega_0, d)} = \frac{\prod_{k=0}^{N-1} \exp(-|r_k - Ae^{j(\omega_0 k+\theta)}c_k|^2/\sigma^2)}{\prod_{k=0}^{N-1} \exp(-|r_k - Ae^{j(\omega_0 k+\theta)}d_k|^2/\sigma^2)} \tag{6}$$

where, r is a vector of received signal, and d is a vector of an ECG signal's symbol, $p_1(r|\theta, \omega_0)$ is the PDF for H1, $p_0(r|\theta, \omega_0, d)$ is the PDF for $H_{0,0}$ and $H_{0,1}$. For $L(r|\theta, \omega_0)$, we will find the expectation about the random variable θ, ω_0, d and get the average likelihood ratio test (ALRT) quantity, as shown in Eq. 7.

$$\mathrm{ALRT}(\Lambda(r)) = \frac{\sum_{q=1}^{N-1}\left|\sum_{q=1}^{N-1} r_k r_{k-q}{}^* c_k{}^* c_{k-q}\right|^2 > H_1}{\sum_{q=1}^{N-1}\left|\sum_{q=1}^{N-1} r_k r_{k-q}{}^* c_k{}^* c_{k-q}\right|^2 < H_{0,0}|H_{0,1}} \lambda \tag{7}$$

ALRT has high computational complexity and is not fit for some of the healthcare applications that have extremely high real-time demands. A simplified version of ALRT is represented using Eq. 8.

$$\Lambda(r) \frac{\sum_{q=1}^{N-1}\left|\sum_{q=1}^{N-1} r_k r_{k-q}{}^* c_k{}^* c_{k-q}\right|^2 > H_1}{\sum_{q=1}^{N-1}\left|\sum_{q=1}^{N-1} r_k r_{k-q}{}^* c_k{}^* c_{k-q}\right|^2 < H_{0,0}|H_{0,1}} \lambda \tag{8}$$

Here, q is the relative delay. In this paper, we discuss how to choose a suitable value of q. Since $\Lambda(r)$ contains a differential correlation term, this simplified method is known as differential correlation detection. The differential correlation detection is relatively easy to implement. Figure 2 shows an implementation structure.

4 Theoretical analysis of our proposed approach

In this section, we derive the missed detection rate and false alarm rate of differential correlation detection for ECG waveform.

4.1 Cumulative probability density function for detection volume

To analyze the cumulative probability density function, the theoretical performance for differential correlation detection needs to be derived. First, we analyze the probability density function of the numerator and denominator of Eq. 8. The numerator can be expressed as:

$$X = \left|\sum_{q=1}^{N-1} r_k r_{k-q}{}^* c_k{}^* c_{k-q}\right|^2 \tag{9}$$

Next, we define

$$U = \frac{1}{N-q} X = \frac{1}{N-q}\left|\sum_{q=1}^{N-1} r_k r_{k-q}{}^* c_k{}^* c_{k-q}\right|^2 = \left|\zeta_q + \xi_q\right|^2 \tag{10}$$

where,

$$\zeta_q = \frac{1}{\sqrt{N-q}} \sum_{q=1}^{N-1} A^2 d_k d_{k-q}{}^* c_k{}^* c_{k-q} e^{-j\omega_0 q} \tag{11}$$

$$\xi_q = \frac{1}{\sqrt{N-q}} \sum_{q=1}^{N-1} {}^* c_k{}^* c_{k-q} (A c_k e^{j\omega_0 k} v_{k-q}^* + A c_{k-q}^* e^{-j\omega_0 (k-q)} v_k + v_k v_{k-q}^*) \tag{12}$$

According to the central limit theorem (CLT), if q is too small, and ξ_q nearly obeys the zero-mean Gaussian distribution, then the variance of σ_ζ^2 is $\sigma_\zeta^2 = \sigma^2(2A^2 + \sigma^2)$. In case of $H_{0,0}$ and H_1, ζ_q is a definite lower variable and we have $\zeta_q = \sqrt{N-q} A^2 e^{-j\omega q}$. For $H_{0,1}$, ζ_q is a random variable that obeys zero-mean Gaussian distribution. In this case, the variance is $\sigma_\zeta^2 = A^4$ which obeys Gaussian distribution. Using the Chi definition, the random variable $U(U|H_1)$ obeys non-central Chi- square distribution with degree of freedom of 2 and non-central parameter of $(N-q)A^4$ under the case of H_1. The random variable $\mathrm{U}(U|H_{0,0})$ obeys central Chi-square distribution with degree of freedom of 2 under the case of $H_{0,0}$.

The definition of denominator of $\Lambda(r)$ is

$$Y = \sum_{k=q}^{N-1} \left|\zeta_{k,q}\right|^2 = \sum_{q=1}^{N\,1} \left|r_k r_{k\,q}{}^* c_k{}^* c_{k\,q}\right|^2 \tag{13}$$

where,

$$\zeta_{k,q} = r_k r_{k\,q}{}^* c_k{}^* c_{k\,q} = e^{j(\theta+\omega_0 q)} c_k{}^* c_{k\,q} (A^2 d_k d_{k\,q}^* + A d_k v_{k\,q}^* + A v_k c_{k\,q}^* + v_k v_{k\,q}^*) \tag{14}$$

For $H_{0,0}$ and H_1, $\zeta_{k,q}$ approximately obeys the mean $\mu_\zeta = e^{j\theta} A^2$, the variance is $\sigma_\zeta^2 = \sigma^2(2A^2 + \sigma^2)$, which is Gaussian distribution. For $\mathrm{H}_{0,1}$, $\zeta_{k,q}$ approximately obeys the mean zero and variance is $\sigma_\zeta^2 = (A^2 + \sigma^2)$ which is Gaussian distribution. This approximation is not strictly true and will lead to some minor deviation between the theoretical analysis and actual performance. However, this

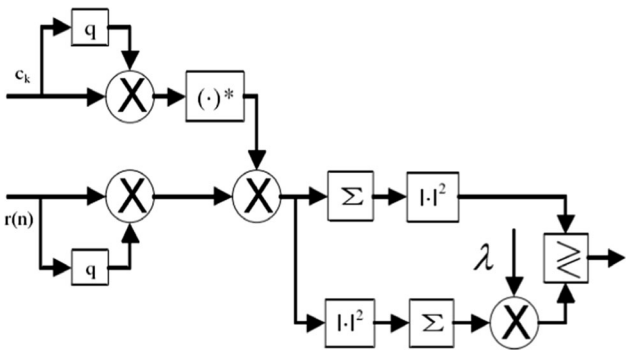

Fig. 2 Implementation structure of differential correlation

deviation is acceptable for performance analysis and will be further discussed in the simulation section.

The random variable $Y(Y|H_1)$ obeys non-central Chi-square distribution with degree of freedom of 2 $(N-q)$ and non-central parameter of $(N-q)A^4$ under the case of H_1. The random variable $\mathrm{Y}(\mathrm{Y}|H_{0,0})$ obeys the central Chi-square distribution and its degree of freedom is $2(N-q)$ under the case of $H_{0,0}$. It must be pointed out that since both Y and X are related to the stochastic vector r, they are not statistically independent. This problem can be solved using Eq. 15.

$$V = Y - U \tag{15}$$

We can prove that V and U are relatively independent.

For $H_{0,0}$ and H_1, the non-central parameters of Y and U correspond to $(N-q)A^4$, $V|H_1$ and $V|H_{0,0}$. They all obey the central Chi-square distribution and its degrees of freedom is $(2(N-q)-2)$. For $H_{0,1}$, since $Y|H_1$ and $V|H_1$ obey the central Chi-square distribution, $V|H_{0,1}$ obeys the central Chi square distribution and its degrees of freedom is $(2(N-q)-2)$. Hence, we define

$$\begin{aligned}\overline{\Omega}(r) =& \frac{U/2}{V/(2(N-q)-2)} \\ =&(N-q-1)\frac{U}{V} = (N-q-1)\Omega(r)\end{aligned} \tag{16}$$

where,

$$\Omega(r) = U/V \tag{17}$$

We know the definition of F-distribution, so the probability density distributions of $H_{0,0}$ and $H_{0,1}$ (represented as $f_{\overline{\Omega}|H_{0,0}}\overline{\Omega}(r)$ and $f_{\overline{\Omega}|H_{0,1}}\overline{\Omega}(r)$ respectively) are the central F-distribution and their degrees of freedom are 2 and $(2(N-q)-2)$, respectively, and the probability is $\overline{\Omega}(r)$ in the case of H_1. The density distribution (denoted as $f_{\overline{\Omega}|H_1}\overline{\Omega}(r)$) is a non-central F-distribution with degrees of freedom 2 and $(2(N-q)-2)$, respectively, and its non-central parameter φ_U is defined as

$$\varphi_U = \frac{2A^4(N-q)}{\sigma^2(2A^2+\sigma^2)} = \frac{2R^2(N-q)}{2R+1} \tag{18}$$

Here, R is the SNR, which is defined as $R = A^2/\sigma^2$. Therefore, the probability density $\Omega(r)$ can be represented as

$$f_{\overline{\Omega}|H}(\Omega(r)) = (N-q-1)f_{\overline{\Omega}|H}((N-q-1)\Omega(r)) \tag{19}$$

where, H represented $H_{0,0}$, $H_{0,1}$, and H_1, respectively. According to Eqs. (10), (15), (17) and (19), the cumulative density function of $\Lambda(r)$ can be expressed as:

$$\begin{aligned}P_H(\Lambda(r)<\lambda) =& P_H\left(\frac{X}{Y}<\lambda\right) \\ =& P_H\left(\frac{U}{V}<\frac{\lambda}{N-q-\lambda}\right) \\ =& P_H\left(\Omega(r)<\frac{\lambda}{N-q-\lambda}\right) \\ =& \int_0^{\frac{\lambda}{N-q-\lambda}} f_{\Omega}(\Omega(r))\mathrm{d}(\Omega(r)) \\ =& \int_0^{\frac{\lambda}{N-q-\lambda}} f_{\overline{\Omega}|H}(\Omega(r))\mathrm{d}(\Omega(r))\end{aligned} \tag{20}$$

4.2 Mathematical expectation for detection threshold

In this section, we derive $H_{0,0}$, $H_{0,1}$, and H_1, i.e., the mathematical expectation for configuring the detection threshold using a large sequence of ECG waveforms. According to the probability density distribution of Eq. 9 and 10, it can be inferred that in the case of H_1, $X/((N-q)\sigma^2/2)$ obeys the non-central Chi-square distribution with $v_x = 2$ degrees of freedom, and its non-central parameters are expressed using Eq. 21.

$$\phi_x = (N-q)A^4/(\sigma^2(2A^2+\sigma^2)/2) \tag{21}$$

In case of $H_{0,0}$, $X/((N-q)\sigma^4/2)$ obeys the non-central Chi-square distribution with $v_x = 2$ degrees of freedom, and in the case of $H_{0,1}$, $X/((N-q)\sigma^4/2)$ also obeys the non-central Chi-square distribution with $v_x = 2$ degrees of freedom. From the statistical characteristics of Chi-square distribution, we know the mean value of X can be represented as

$$m_{x|H_{0,0}} = v_x(N-q)\sigma^4/2 = (N-q)\sigma^4 \tag{22}$$

$$\begin{aligned}m_{x|H_{0,1}} =& v_x(N-q)(A^2+\sigma^2)^2/2 \\ =&(N-q)(A^2+\sigma^2)^2\end{aligned} \tag{23}$$

$$\begin{aligned}m_{x|H_1} =& (v_x+\phi_x)(N-q)\sigma^2(2A^2+\sigma^2)/2 \\ =&(N-q)(\sigma^2(2A^2+\sigma^2)+(N-q)A^4)\end{aligned} \tag{24}$$

The variance of X is:

$$\begin{aligned}\sigma^2_{x|H_{0,0}} =& 2v_x((N-q)\sigma^4/2)^2 \\ =&(N-q)^2\sigma^8\end{aligned} \tag{25}$$

$$\begin{aligned}\sigma^2_{x|H_{0,1}} =& 2v_x((N-q)(A^2+\sigma^2)^2/2)^2 \\ =&(N-q)^2(A^2+\sigma^2)^4\end{aligned} \tag{26}$$

$$\begin{aligned}\sigma_{x|H_1} =& 2(v_x+2\phi_x)((N-q)\sigma^2(2A^2+\sigma^2)/2)^2 \\ =&(N-q)^2\sigma^2(2A^2+\sigma^2)(2\sigma^2(2A^2+\sigma^2)+2(N-q)A^4)\end{aligned} \tag{27}$$

According to the probability density distribution of (13) and Y, it can be inferred: in the case of H_1, $Y/(\sigma^2(2A^2+\sigma^2)/2)$ obeys the non-central Chi-square distribution with $v_Y = 2(N-q)$ degrees of freedom, and the non-central parameters are:

$$\phi_Y = (N-q)A^4/(\sigma^2(2A^2+\sigma^2)/2) \tag{28}$$

In the case of $H_{0,0}$, $Y/(\sigma^4/2)$ obeys the central Chi-square distribution with the degree of freedom $v_Y = 2(N-q)$. In the case of $H_{0,1}$, $Y/((A^2+\sigma^2)/2)$, also obeys the central Chi-square distribution of F. By the statistical characteristics of Chi-square distribution, the mean value of Y can be expressed as

$$m_{Y|H_{0,0}} = v_Y\sigma^4/2 = (N-q)\sigma^4 \tag{29}$$

$$\begin{aligned} m_{Y|H_{0,1}} =& v_Y(A^2+\sigma^2)^2/2 \\ =& (N-q)(A^2+\sigma^2)^2 \end{aligned} \tag{30}$$

$$\begin{aligned} m_{Y|H_1} =& (v_x+\phi_Y)\sigma^2(2A^2+\sigma^2)/2 \\ =& (N-q)(\sigma^2(2A^2+\sigma^2)+A^4) \end{aligned} \tag{31}$$

The variance of Y is expressed as

$$\sigma^2_{Y|H_{0,0}} = 2v_Y(\sigma^4/2)^2 = (N-q)^2\sigma^8 \tag{32}$$

$$\begin{aligned} \sigma^2_{x|H_{0,1}} =& 2v_x((N-q)(A^2+\sigma^2)^2/2)^2 \\ =& (N-q)^2(A^2+\sigma^2)^4 \end{aligned} \tag{33}$$

$$\begin{aligned} \sigma_{Y|H_1} =& 2(v_Y+2\phi_Y)(\sigma^2(2A^2+\sigma^2)/2)^2 \\ =& (N-q)^2\sigma^2(2A^2+\sigma^2)(2\sigma^2(2A^2+\sigma^2)+2A^4) \end{aligned} \tag{34}$$

From Eqs. 32–34, we can conclude that

$$\sigma^2_{x|H_{0,0}}/\sigma^2_{Y|H_{0,0}} >> 1, \sigma^2_{x|H_{0,1}}/\sigma^2_{Y|H_{0,1}} >> 1, \sigma^2_{x|H_1}/\sigma^2_{Y|H_1} >> 1$$

Based on this conclusion, the denominator Y can be approximated with deterministic variables while calculating the expectation of ALRT ($\Lambda(r)$). Therefore:

$$E\{\Lambda(r)|H_{0,0}\} \approx m_{x|H_{0,0}}/m_{Y|H_{0,0}} = 1 \tag{35}$$

$$E\{\Lambda(r)|H_{0,1}\} \approx m_{x|H_{0,1}}/m_{Y|H_{0,1}} = 1 \tag{36}$$

$$\begin{aligned} E\{\Lambda(r)|H_1\} \approx& m_{x|H_1}/m_{Y|H_1} \\ =& \frac{(N-q)(\sigma^2(2A^2+\sigma^2)+(N-q)A^4)}{(N-q)(\sigma^2(2A^2+\sigma^2)+A^4)} \\ =& \frac{\frac{(2R+1)}{R^2}+(N-q)}{\frac{(2R+1)}{R^2}+1} < N-q \end{aligned} \tag{37}$$

Here, R is big enough to accommodate the large volume of waveforms generated by ECG signals, Using Eq. 37, we can easily set the detection threshold.

4.3 Missing detection rate and false alarm rate of differential correlation detection

The missing detection rate is defined as:

$$P_m(\lambda) = P_{H_1}(\Lambda(r) \le \lambda) \tag{38}$$

According to the discussion in Sect. 3.1 and Eq. 20, the above equation can be further written as:

$$\begin{aligned} P_m(\lambda) =& \int_0^{\frac{\lambda}{N-q-\lambda}} f_{\overline{\Omega}|H_1}(\Omega(r))\mathrm{d}(\Omega(r)) \\ =& Q_{\mathrm{NCF}}(\frac{(N-q-\lambda)\lambda}{N-q-\lambda}, 2, 2(N-q)-2, \phi_U) \end{aligned} \tag{39}$$

where, $Q_{\mathrm{NCF}}(\rho, v_1, v_2, \delta_1)$ is the degree of freedom v_1 and v_2, i.e., the non-central F distribution whose non-central parameter is δ_1 can be expressed as:

$$Q_{\mathrm{NCF}}(\rho, v_1, v_2, \delta_1) = \sum_{j=0}^{\infty}\left(\frac{(\frac{\delta_1}{2})^j}{j!}e^{-\frac{\delta_1}{2}}\right) I\left(\frac{v_1\rho}{v_1+\rho v_1}, \frac{v_1}{2}+j, \frac{v_2}{2}\right) \tag{40}$$

where, $I(\cdot)$ is the incomplete β function, its definition is:

$$I(\lambda, v_1, v_2) = \frac{1}{B(v_1, v_2)}\int_0^{\lambda} t^{v_1-1}(1-t)^{v_2-1}\mathrm{d}t \tag{41}$$

The false alarm probability of detection is defined using Eq. 42.

$$P_f(\lambda) = P_{H_{0,0}}P_{f|H_{0,0}}(\lambda) + P_{H_{0,1}}P_{f|H_{0,1}}(\lambda) \tag{42}$$

Here, $P_{H_{0,0}}$ represents the probability of $H_{0,0}$, $P_{f|H_{0,0}}(\lambda)$ represents the false alarm probability caused by the noise part, $P_{H_{0,1}}$ represents the probability of $H_{0,1}$, $P_{f|H_{0,1}}(\lambda)$ represents the false alarm probability caused by the ECG signal, i.e., the original waveform.

According to the discussion in Sect. 3.1, in case of $H_{0,0}$ and $H_{0,1}$, the cumulative probability density function of the detection quantity is the same, therefore,

$$P_{f|H_{0,1}}(\lambda) = P_{f|H_{0,1}}(\lambda) \tag{43}$$

Definition: $P_{H_0} = P_{f|H_{0,1}}(\lambda) = P_{f|H_{0,0}}(\lambda)$ then:

$$P_f(\lambda) = P_{H_0}(\Lambda(r) > \lambda) = 1 - P_{H_0}(\Lambda(r) \le \lambda) \tag{44}$$

Using the discussion results of Eq. 20 and Sect. 3.1, the above equation can be further expressed as:

$$\begin{aligned} P_f(\lambda) =& \int_0^{\frac{(N-q-\lambda)\lambda}{N-q-\lambda}} f_{\overline{\Omega}|H_1}(\Omega(r))\mathrm{d}(\Omega(r)) \\ =& \left(1-\frac{\lambda}{N-q}\right)^{N-q-1} \end{aligned} \tag{45}$$

5 The proposed deep neural network-based classifiers

We use two different ML classifiers: (i) Long Short-Term Memory (LSTM); and (ii) Convolutional Neural Network (CNN) to categorize various heart diseases using the ECG signals. In the rest of this section, we briefly describe these models.

5.1 Long short-term memory (LSTM)

We classified the ECG signals based on Convolutional neural networks and LSTM. LSTM is a time-recurrent neural network. It is suitable for time-series prediction of important events, and the delay interval is relatively long. Neural network can effectively retain historical information and realize learning of long-term dependence information of signals (text). The LSTM network consists of an input gate, forget gate, output gate, and a cell unit to update and retain historical information. Figure 3 shows a ConvLSTM block. For every heartbeat, the input ECG samples along with the extracted interval features and wavelet features are provided to two separate ConvLSTM models. The two models make separate arrhythmia predictions which are then blended to form the final prediction for every heartbeat. Further, additional features of the signal may help the ConvLSTM models to capture patterns in the ECG signals more efficiently. The additional features provide processed information to the accurate LSTM models. Therefore, results can be reached with smaller and, hence, faster. Employing multiple smaller LSTMs in parallel instead of one larger LSTM helps to increase the accuracy without significantly increasing the computational costs. In the above simple RNN cell the effect of all previous information is accumulated in the internal state vector. Gradient-based algorithms may fail when temporal dependencies get too long because gradient values may increase or decrease exponentially.

LSTM solves this issue by allowing to forget according to the actual dependencies which exist in the problem. The dependencies are automatically extracted based on the data. This is achieved through forget, input and output gates the LSTM cell. As the above equations show, the LSTM output still depends on all previous inputs. Previous information is neither completely discarded nor completely carried over to the current state. Instead, influence of the previous information on the current state is carefully controlled through the gate signals. Forget gate ft in the LSTM memory block is controlled by a simple single neuron. It determines which information must be retained or discarded to enable the storage of historical information. Input gate it is a section where the LSTM block is created by a neuron and previous memory unit effects. It is activated to determine whether to update the historical information to the LSTM block. Candidate update content c_{in} is calculated by a tan$h$ neuron. Current time memory cell state value c_t is calculated from the current candidate cell c_{in}, the previous time state $c_t - 1$, the input gate information it, and the forget gate information f_t, o_t of the LSTM block at the current time is generated at the output gate. Finally, a_t determines the amount of information about the current cell state that will be output. Activation of each gate and the update of the current cell state can be calculated as follow. The mathematical formulation for LSTM is as follows.

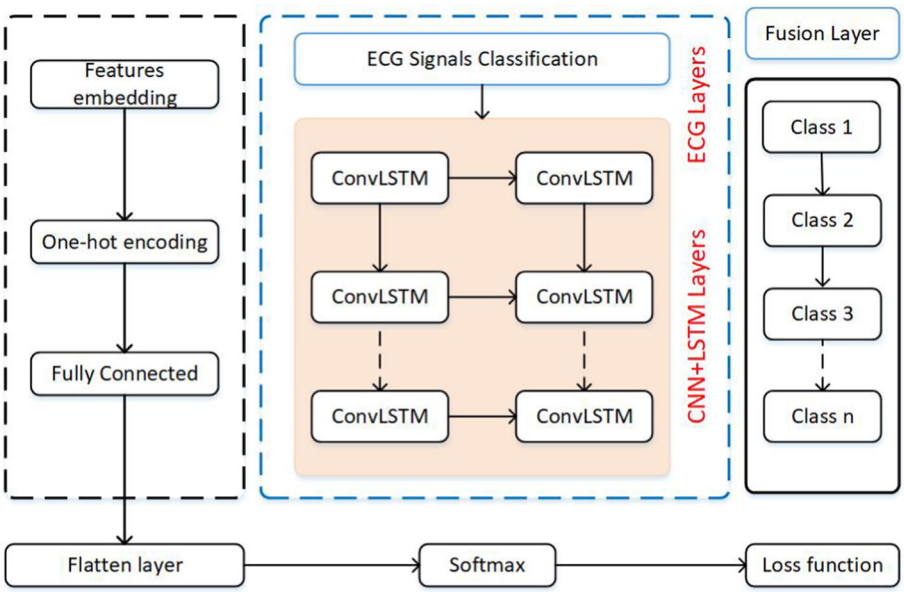

Fig. 3 The proposed deep learning-based classifier for the heartbeat signals

$$i_t = O(W_{xt} * X_{ct} + W_{ht} * X_{ct-1} + W_{ct} * X_{ct-1} + b_t) \quad (46)$$

$$f_t = O\big(W_{xf} * X_{cf} + W_{hf} * X_{cf-1} + W_{cf} * X_{cf-1} + b_f\big) \quad (47)$$

$$c_t = O(W_{xc} * X_{cc} + W_{hc} * X_{cc-1} + W_{cc} * X_{cc-1} + b_c) \quad (48)$$

$$o_t = O(W_{xo} * X_{co} + W_{ho} * X_{co-1} + W_{co} * X_{co-1} + b_o) \quad (49)$$

In this paper, we use the four-layer LSTM architecture including an input layer, an LSTM layer, and two fully connected layers. structure of the proposed LSTM for imbalanced ECG signal feature extraction and classification tasks.

5.2 Convolutional neural network and gated recurrent unit

The deep neural network (DNN) is extensively used in different kinds of applications. CNN [31] is one of the most powerful DNNs for videos and image processing. For urban crowd flows predictions problem, firstly use CNN model to extract the spatial data from trajectories GPS data. CNN is very good in spatial data extraction, while GPS trajectories data different from manually images because it includes temporal information which directly affect the prediction accuracy. For accurately explore the temporal information, we consider recurrent neural network (LSTM) to simultaneously capture the temporal information. However, the RNN face the problem of vanishing gradient in various kinds of applications. Currently the GRU deal with standard RNN to solve the vanishing gradient problem as well as perform to explore the time series features for a time span. The primary components of our network are GRU combine with CNN which replace the kernel size with convolutional. Our network focuses on hidden features to captures burst information in the ECG signals. The deep hybrid neural network proposed by us, first we divide the DNN into two sub-DNN. The first one captures the spatial features through CNN, while the second learn temporal features over a span of time through GRU.

6 Simulation results and their analysis

In this section, we present the simulation results for the ECG curve using the differential correlation detection. The simulated burst signal is a QPSK burst signal. In the simulation, preambles of different lengths are used, message signs are randomly generated in the modulation signs set, and the noise part is generated with the White Gaussian noise model. The simulation time for evaluating the false alarm rates is set at 1e + 8 time, but when the number of false alarms reaches 20, the simulation terminates. The missed detection rate is a ratio of the number of missed detections to the total number of simulations. The false alarm rate, on the other hand, is a ratio of the number of false alarms to all the count of simulations. We first evaluate the relationship between missed detection rate, false alarm rate, and frequency deviation for an ECG waveform. In this simulation, the preamble length is set to 32, the SNR is set to 5.5 dB, and the detection threshold is set to 16.

After detecting the burst from the ECG signal, we used machine learning models to classify the original and modified signals into various types of heart diseases. We implemented all experiments using (python through Keras and backend Theano libraries) which is the most significant open source framework for deep learning. We used a dataset that consists of various ECG signals generated randomly. The ECG signals were, then, translated to binary form using the most widely used thresholding technique. Furthermore, the testing data are assumed as the last 10% ECG signals and all the remaining data were assumed as a training dataset. To measure the performance of the proposed models, we use Root Mean Square Error (RMSE) and Mean Average Percentage Error (MAPE) metrics. These two metrics are popular in machine learning environment that extensively measure the performances of all learning methods. Particularly, these metrics are defined as follows:

$$\text{RMSE} = \sqrt{\frac{1}{X}\sum_{i=1}^{x}(Yt - Yt)} \quad (50)$$

$$\text{MAPE} = \sqrt{\frac{1}{X}\sum_{i=1}^{x}|Yt - Yt|} \quad (51)$$

In Sect. 5.1, we describe the results of using the burst detection technique; while in Sect. 5.2, we illustrate how the original (with burst) and modified (no burst) ECG signals are classified to various types of heart diseases.

6.1 Burst detection

The simulation results are shown in Fig. 4. It can be seen from this figure that if the normalized frequency offset raises from 0 to 0.5, the missed detection rate and false alarm rate see little fluctuation. In other words, the differential correlation detection has a very strong frequency offset for a given waveform.

Next, we evaluate the relationship between false alert rate, missed detection rate, and SNR. The length of leading header is set to 32, and the detection threshold is set to 16. The simulation results and theoretical analysis results are shown in Fig. 5. It can be seen from the figure that there is a difference between the performance curve of theoretical analysis and the curve of simulation performance, however, the difference is within 0.5 dB. The reason for this

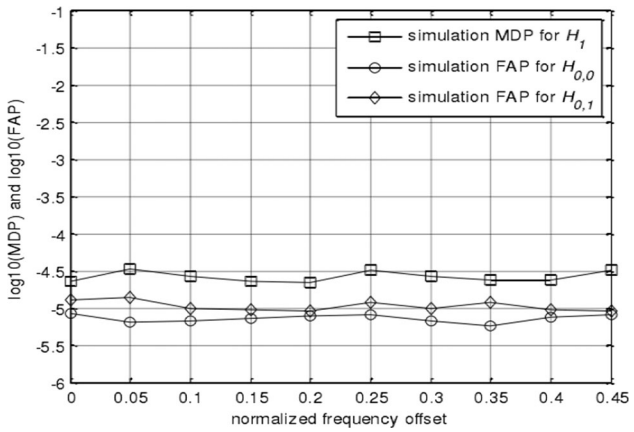

Fig. 4 False alarm rate and missed detection rate under different frequency deviations(R = 5.5 dB, N = 32, λ = 10)for an ECG Waveform

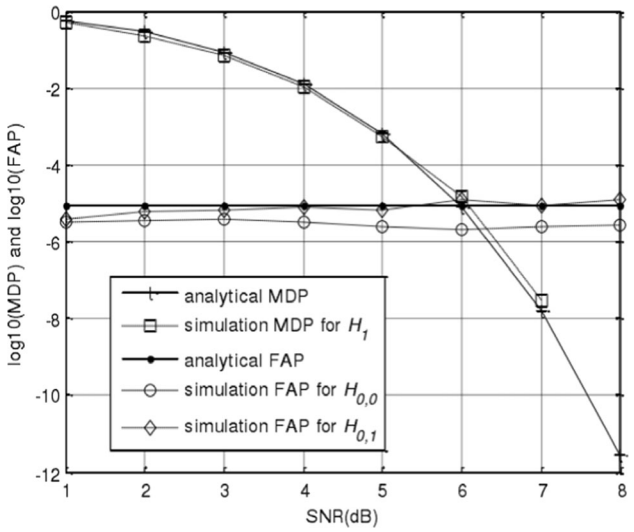

Fig. 5 Missed detection rate and false alarm rate under different SNR(N = 32, λ = 10)for an ECG Waveform

difference is that the probability distribution of variables is approximated in the theoretical analysis. This small difference is acceptable for performance evaluation, especially when the SNR is too low. This figure also shows that the false alarm rate in the case of $H_{0,0}$ is equivalent to the false alarm rate of $H_{0,1}$, especially when the SNR is low. In addition, both the performance curve of theoretical analysis and the curve of simulation performance show that the differential correlation detection is a common false alarm detection approach, and the missed detection rate decreases as the SNR increases.

Similar to any other application, the threshold under given conditions is an important focus of performance analysis in healthcare. Through theoretical analysis and simulation analysis of the relationship between false alarm rate, missed detection rate and detection threshold under typical conditions, it can provide reference for threshold setting. In this simulation, the leading header length is set to 16, 32, and 64, respectively. Figure 5 shows the ROC curve (receiver operating characteristic curve) of differential correlation detection when the SNR is 6 dB and the leading length is 16. Figure 7 shows the differential correlation detection when the SNR is 9 dB and the leading length is 16. In Fig. 8, the ROC curve of differential correlation detection when the SNR is 2 dB and the leading length is 32 is shown. Figure 9 shows the differential correlation detection when the SNR is 8 dB and the leading length is 32. Figure 10 shows the ROC curve of differential correlation detection when the SNR is 1 dB and the leading length is 64. Figure 10 shows the differential correlation detection when the SNR is 4 dB and the leading length is 64. From these curves (Fig. 6, 7, 8, 9, 10 and 11), it is obvious that simulation curves are very close to the theoretical analysis. Besides, these figures once again confirm that the false alert rate of $H_{0,0}$ is equivalent to that of $H_{0,1}$. These analysis results provide a reference for the detection threshold setting, to satisfy the performance trade-off demands of any healthcare system for false alarm rate and the missed detection rate.

Figure 12 and 13, respectively, show the health monitoring process of Subject No. 1 and Subject No. 2. The waveform in (a) represents the movement of the subject's center of gravity, that is, the angle between the plumb line and the torso (B) represents the motion signal obtained after (a) wavelet decomposition and reconstruction processing; (c) represents the real-time motion signal of the subject's knee joint, which is the subject's motion; (d) Represents (c) the motion signal obtained after wavelet decomposition and reconstruction processing. It can be found that the signal after wavelet decomposition and reconstruction processing is smoother, reducing signal

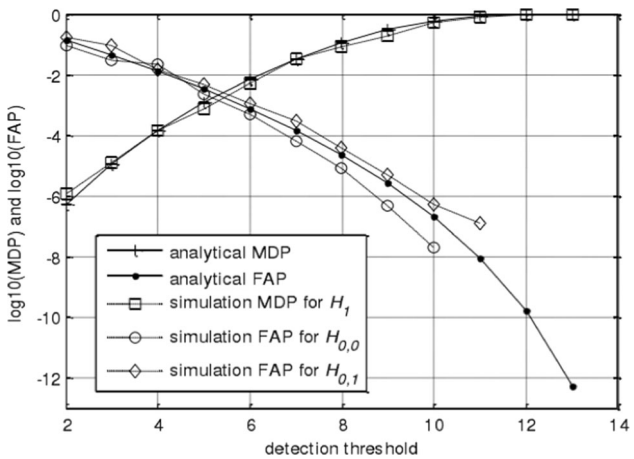

Fig. 6 ROC curve when the SNR is 6 dB and the leading length of a waveform is 16

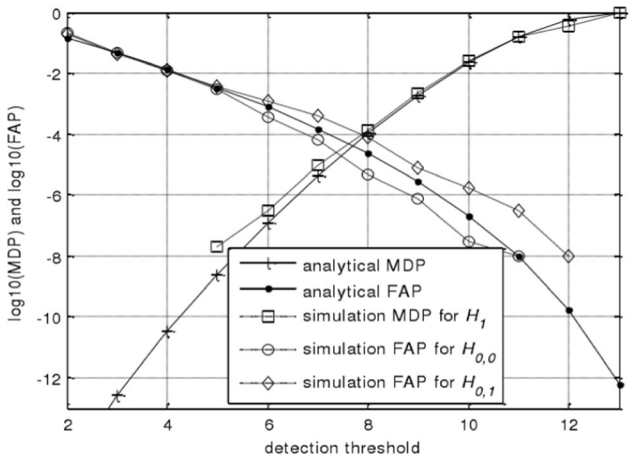

Fig. 7 ROC curve when the SNR is 9 dB and the leading length of a waveform is 16

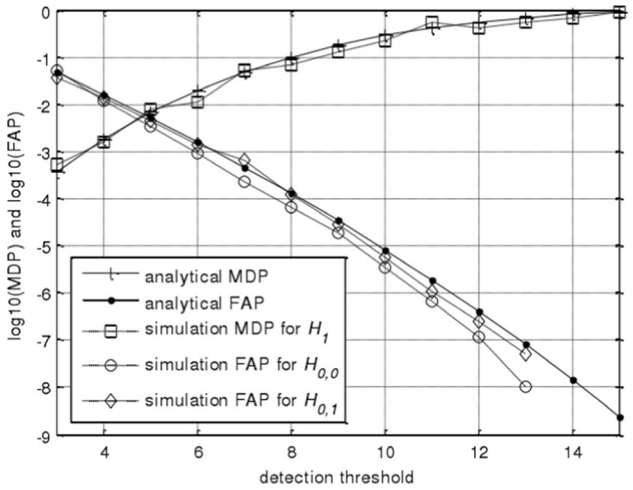

Fig. 8 ROC curve when the SNR is 2 dB and the leading length of a waveform is 32

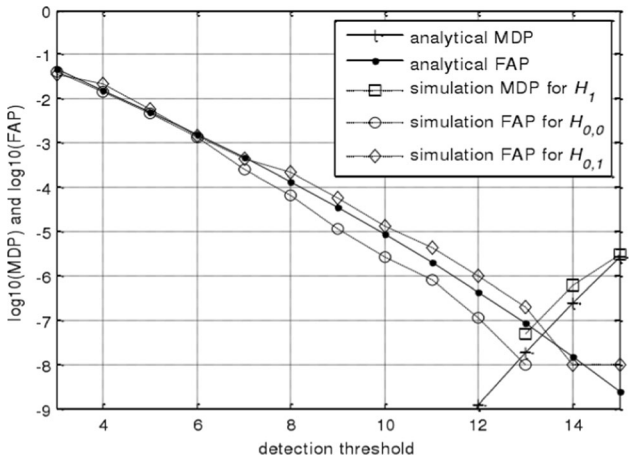

Fig. 9 ROC curve when the SNR is 8 dB and the leading length of a waveform is 32

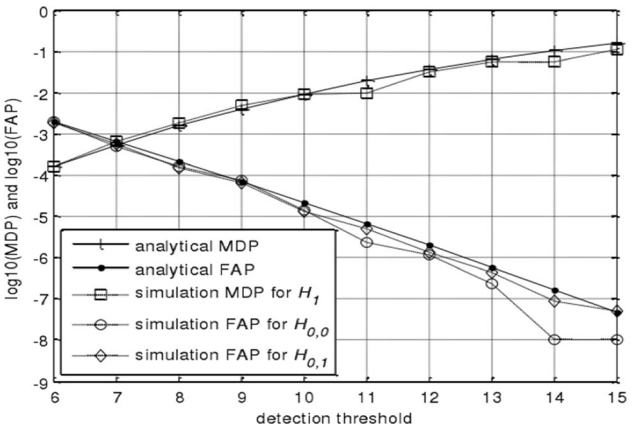

Fig. 10 ROC curve when the SNR is 1 dB and the preamble length of a waveform is 64

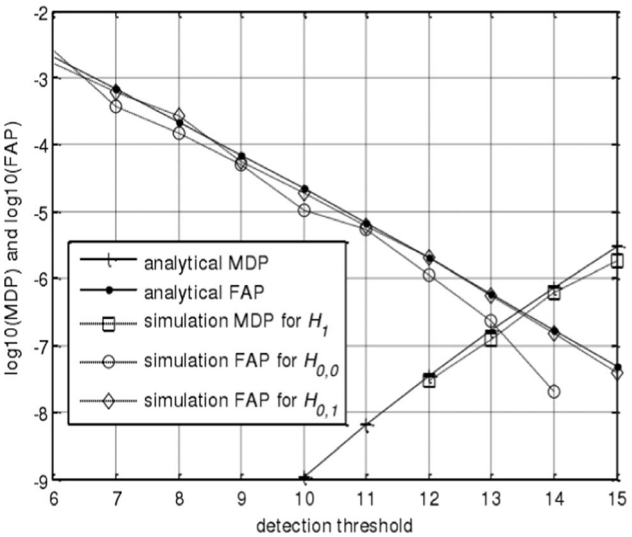

Fig. 11 ROC curve when the SNR is 4 dB and the preamble length of a waveform is 64

jitter and glitches, that is, it can effectively suppress the motion process noise interference.

According to the comparison between Fig. 12b and 13b, it can be seen that the signal peak in Fig. 8b is more stable, which indicates that the center of gravity of subject No. 1 can well assist the hip-knee-ankle during the monitoring process. Movement; comparing Fig. 12d with Fig. 13d, the hip-knee-ankle motion signal in Fig. 12d is smoother than the hip-knee-ankle motion signal in Fig. 13d. Through a simple analysis of the motion waveforms of the two subjects, it is concluded that the exercise completed by the first subject during the knee health monitoring period is better than that of the second subject.

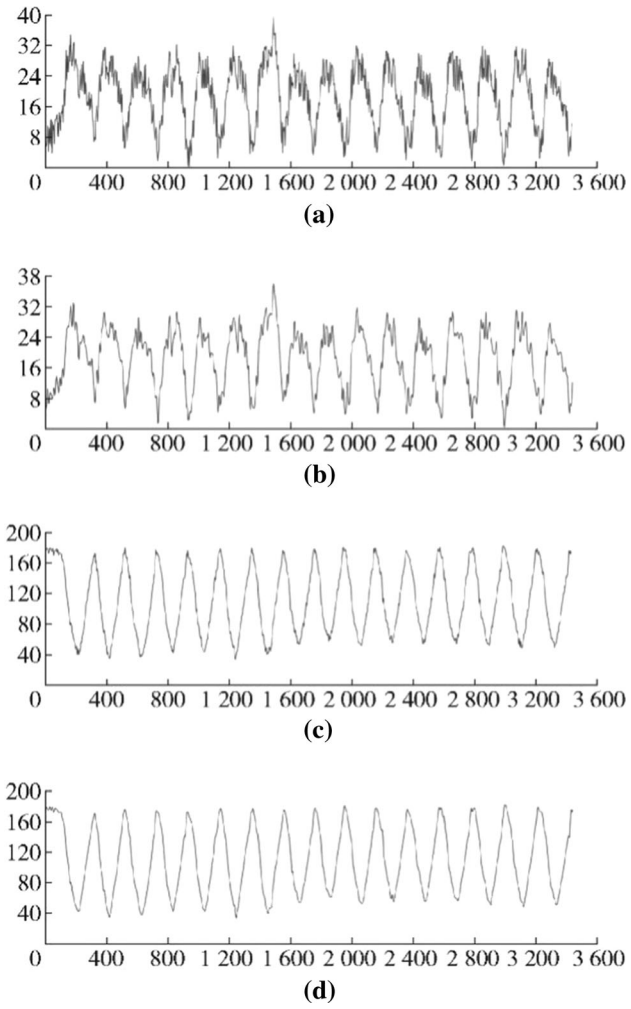

Fig. 12 Signal map of tester 1 after deep learning

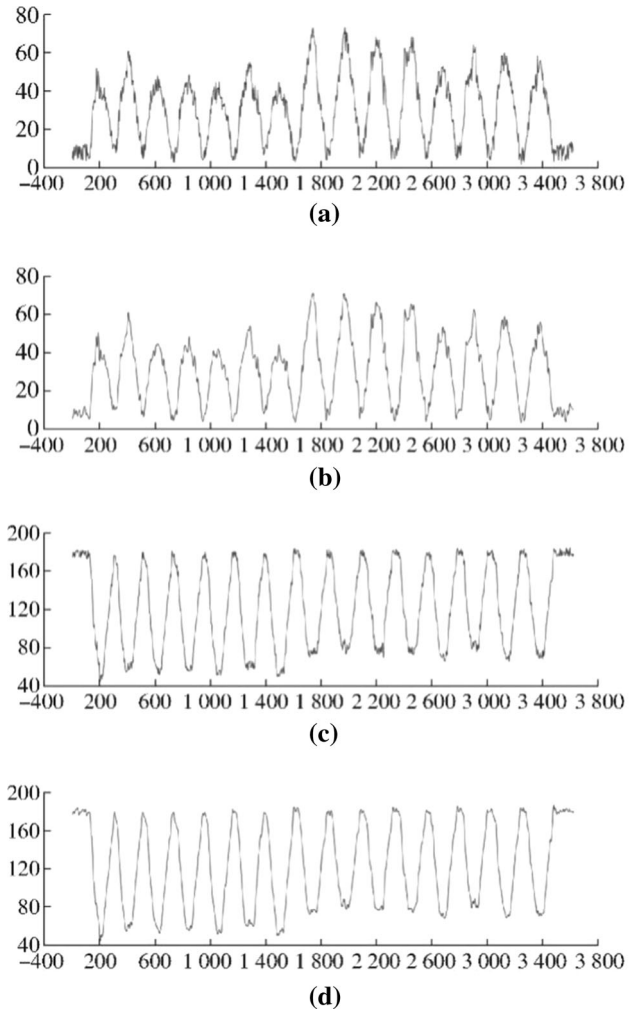

Fig. 13 Signal map of tester 2 after deep learning

6.2 Machine learning based classification of the ECG signals

Figures 14 and 15 show the mean results (across 10 experiments with different datasets) of our proposed model to classify the ECG signal to four different types of the heart diseases, as described earlier. We determine the RMSE values for different classes using two different approaches of deep learning: (i) LSTM; and (ii) CNN. By using the LSTM model, all classes' show better performance; however, using the CNN model the accuracy of class 4 is a little bit lower than the other three classes. This is potentially, due to the fact, that the bursting method was unable to accurately filter the signals. We observed that lower accuracy was deviated more from the means as compared to the higher accuracy. For example, using the LSTM approach, the RMSE for the class 1 disease was noted 92.82 ± 1.09; however, for class 4 disease this value was noted as 85.01 ± 5.78 (the ± shows the standard deviation). Similarly, using the CNN approach, the RMSE

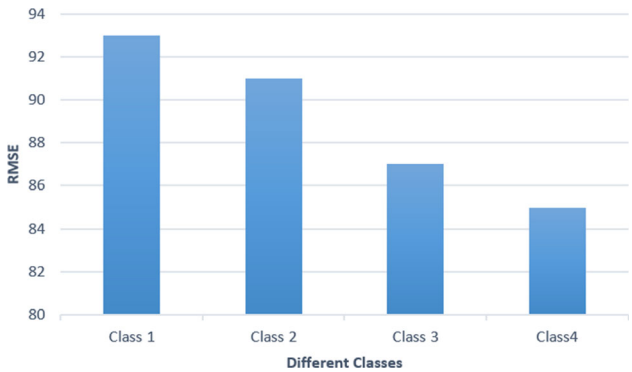

Fig. 14 Results of different classes classification (using LSTM)

for the class 1 disease was noted 90.12 ± 1.39; however, for class 4 disease this value was recorded as 77.81 ± 9.12. For certain diseases, LSTM outperformed the CNN model while for other, the opposite was observed—as shown in Fig. 14 and 15.

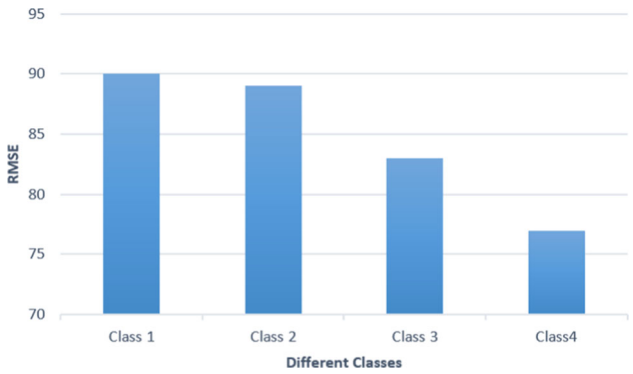

Fig. 15 Results of different classes classification (using CNN)

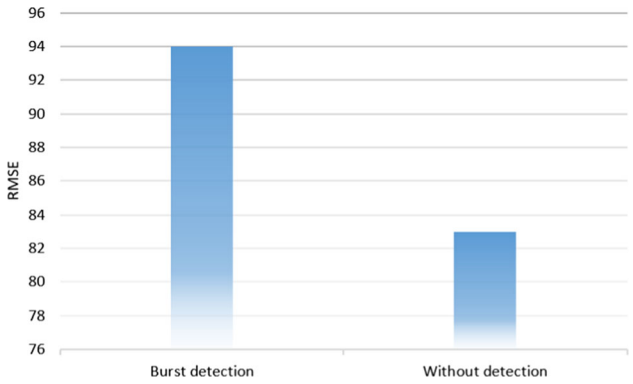

Fig. 16 Results of RMSE (using LSTM)

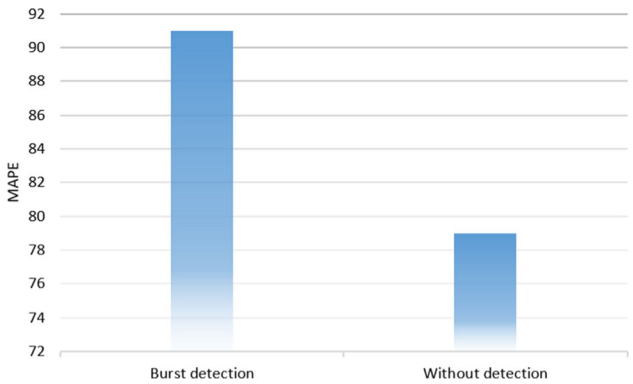

Fig. 17 Results of MAPE (using LSTM)

Similarly, Figs. 16 and 17 show results of both ECG signals i.e., with burst (original) and without burst detection (modified signal). By using the RMSE and MAPE metrics and their values as shown in Fig. 16 and 17, the accuracy of the former approach (with burst detection) is much better than the later one i.e., without burst detection. It shows that, the accuracy is much important in burst detection technique by using the above two metrics. For example, the RMSE and MAPE accuracy of the LSTM based ECG signal classification could be approximately 11.7% and 12.8%, subsequently, improved using the proposed burst detection method. Larger accuracy values were noticed for the CNN model that could be related incrementally with the disease classes. This shows the significance of the proposed burst detection technique.

7 Conclusion and future work

In this paper, we discussed the performance of differential correlation detection for massive ECG waveforms by deriving closed-form analytical expressions for false alarm rate and missed detection rate with deep learning. Our proposed approach is extremely beneficial for the public health and safety to ensure that burst and noise are removed from ECG waveforms. Unlike the existing studies, we considered false alarm rate for noise as well as message signal segment, which contain vital information in an ECG waveform. Based on our analysis and experimental results, the false alarm rate is approximately similar to its counterpart for the message signal segment. Meantime by the simulation results with deep learning frame, we also verify the theoretical analysis results. Both simulation and theoretical analysis show that the differential correlation detection has excellent characteristics such as robustness to frequency deviation, constant false alert, and the detection threshold. These characteristics mean that the differential correlation detection way is very functional for burst detection applications. These analysis results also provide a reference for how to set the detection threshold to satisfy the system performance requirements under different conditions. In the future, our aim would be to develop a cloud-based system that can check the real-time heart disease detection. If we implement the training module on the cloud and then the prediction model is implemented on the edge computing or a small datacenter, then the benefit is that each physician should quickly monitor, predict and take appropriate decisions for patients' health monitoring and diagnosis. For that we will need to deploy fog devices in local hospitals, etc. which are connected to a remote cloud system.

Acknowledgements Taif University Researchers Supporting Project number (TURSP-2020/126), Taif University, Taif, Saudi Arabia

Compliance with ethical standards

Conflicts of interest The authors declare no conflict of interest.

References

1. Guo F, Wan W, Yu X (2019) Performance analysis of a differential-correlation based burst detection method. Wireless Personal Commun 107(2):1171–1186

2. Song J, Zhang C, Peng K, Wang J, Pan C, Yang F, Wang J, Yang H, Xue Y, Zhang Y, Yang Z (2018) Key technologies and measurements for DTMB-A system. IEEE Trans Broadcast 65(1):53–64
3. Khalifa, A.H., Shehata, M.K., Gasser, S.M. and El-Mahallawy, M.S., 2020. Enhanced cooperative behavior and fair spectrum allocation for intelligent IoT devices in cognitive radio networks. *Phys Commun*, *43*, p.101190.
4. Sodhro AH, Malokani AS, Sodhro GH, Muzammal M, Zongwei L (2020) An adaptive QoS computation for medical data processing in intelligent healthcare applications. Neural Comput Appl 32(3):723–734
5. Satija U, Ramkumar B, Manikandan MS (2017) Automated ECG noise detection and classification system for unsupervised healthcare monitoring. IEEE J Biomed Health Inform 22(3):722–732
6. Yu X, Jiang F, Du J, Gong D (2019) A cross-domain collaborative filtering algorithm with expanding user and item features via the latent factor space of auxiliary domains. Pattern Recogn 94:96–109
7. Yu X, Chu Y, Jiang F, Guo Y, Gong D (2018) SVMs classification based two-side cross domain collaborative filtering by inferring intrinsic user and item features. Knowl Based Syst 141:80–91
8. Wang H, Jiang H, Gong K (2020) ML-based forward symbol timing offset estimation for burst signals. IEEE Access 8:200875–200882
9. Yuan-Ling H (2010) Robust burst detection based on the average likelihood ratio test. J Elect Inf Technol 32(2):345–349
10. Bethencourt J, Sahai A, Waters B (2007) Ciphertext-policy attribute-based encryption. In: IEEE symposium on security and privacy (SP'07), Berkeley, pp 321–334.
11. Chase M (2007) Multi-authority attribute based encryption. Lecture notes in computer science, vol 4392. Springer, Berlin, pp 515–534.
12. Hur J, Noh DK (2011) Attribute-based access control with efficient revocation in data outsourcing systems. IEEE Trans Parallel Distrib Syst 22(7):1214–1221
13. Green M, Ateniese G (2007) Identity-based proxy re-encryption. Lecture notes in computer science, vol 4521. Springer, Berlin, pp 288–306.
14. Mizuno T, Doi H. Secure and efficient IBE-PKE proxy re-encryption. IEICE Trans Fundam Elect Commun Comput Sci, 2011, 94(1):36–44.
15. Zhao J, Feng DG, Yang L et al (2011) CCA-secure type-based proxy re-encryption without pairings. Acta Elect Sin 39(11):2513–2519
16. Wu XX, Xu L, Zhang XW (2011) A certificateless proxy re-encryption scheme for cloud-based data sharing. In: The 18th ACM conference on computer and communications security (CCS), pp 869–871.
17. Liang KT, Liu JK, Wong DS, et al (2014) An efficient cloud-based revocable identity-based proxy re-encryption scheme for public clouds data sharing. In: The 19th European symposium on research in computer security (ESORICS), pp 257–272.
18. Yang G, Jan MA, Menon VG, Shynu PG, Aimal MM, Alshehri MD (2020) A centralized cluster-based hierarchical approach for green communication in a smart healthcare system. IEEE Access.
19. Wang C, Wang Q, Ren K, et al (2010) Privacy-preserving public auditing for data storage security in cloud computing. In: The 29th IEEE Infocom, pp 1–9.
20. Yang K, Jia X (2013) An efficient and secure dynamic auditing protocol for data storage in cloud computing. IEEE Trans Parallel Distrib Syst 24(9):1717–1726
21. Li N, Li T, Venkatasubramanian S (2007) T-Closeness: privacy beyond k-anonymity and l-diversity. In: The 23rd IEEE international conference on data engineering (ICDE), pp 6–115.
22. Elkhodr M, Alsinglawi B, Alshehri M (2019) A privacy risk assessment for the internet of things in healthcare. In: Applications of intelligent technologies in healthcare (pp. 47–54). Springer, Cham.
23. Sandhu RS, Coyne EJ, Feinstein HL et al (2009) Role-based access control models. Ansi Incits 4(3):554–563
24. Ray I, Kumar M, Yu L (2006) LRBAC: a location-aware role-based access control model. In: The 2nd international conference on information systems security, pp 147–161.
25. Taha B (2017) Deep learning network for ECG signals classification. The University of Idaho